

Non-Dirac topological surface states in $(\text{SnTe})_{n \geq 2}(\text{Bi}_2\text{Te}_3)_{m=1}$

S. V. Eremeev

*Institute of Strength Physics and Materials Science, 634021, Tomsk, Russia
Tomsk State University, 634050 Tomsk, Russia and
Saint Petersburg State University, Saint Petersburg, 198504, Russia*

T. V. Menshchikova and I. V. Silkin

Tomsk State University, 634050 Tomsk, Russia

M. G. Vergniory

*Donostia International Physics Center (DIPC),
20018 San Sebastián/Donostia, Basque Country, Spain*

P. M. Echenique

*Donostia International Physics Center (DIPC),
20018 San Sebastián/Donostia, Basque Country, Spain
and
Departamento de Física de Materiales UPV/EHU,
Centro de Física de Materiales CFM - MPC and Centro Mixto CSIC-UPV/EHU,
20080 San Sebastián/Donostia, Basque Country, Spain*

E. V. Chulkov

*Donostia International Physics Center (DIPC),
20018 San Sebastián/Donostia, Basque Country, Spain*

*Departamento de Física de Materiales UPV/EHU,
Centro de Física de Materiales CFM - MPC and Centro Mixto CSIC-UPV/EHU,
20080 San Sebastián/Donostia, Basque Country, Spain
Tomsk State University, 634050 Tomsk, Russia and
Saint Petersburg State University, Saint Petersburg, 198504, Russia*

A new type of topological spin-helical surface states was discovered in layered van der Waals bonded $(\text{SnTe})_{n=2,3}(\text{Bi}_2\text{Te}_3)_{m=1}$ compounds which comprise two covalently bonded band inverted subsystems, SnTe and Bi_2Te_3 , within a building block. This novel topological states demonstrate non-Dirac dispersion within the band gap. The dispersion of the surface state has two linear sections of different slope with shoulder feature between them. Such a dispersion of the topological surface state enables effective switch of the velocity of topological carriers by means of applying an external electric field.

PACS numbers: 71.20.Nr, 73.20.At, 85.75.-d

INTRODUCTION

A topological insulators (TIs) are materials with a gap in bulk electronic spectrum driven by the spin-orbit interaction (SOI), which is topologically distinct from the ordinary insulators. This distinction, characterized by a \mathbb{Z}_2 topological invariant, is manifested in the existence of the time-reversal-symmetry protected spin-helical gapless surface state having linear (or almost linear) Dirac dispersion.

Starting from the discovery of the TI phase in the quintuple layer (QL) structured binary compounds Bi_2Te_3 , Bi_2Se_3 , and Sb_2Te_3 and its thorough experimental and theoretical investigation [1–9] a huge number of \mathbb{Z}_2 TIs were found. The most of known TIs are Bi_2Te_3 -type ternary and quaternary layered materials. Among them QL and septuple layer (SL) structured compounds as well as the materials with alternating QL and SL units were theoretically predicted and experimentally confirmed.[10–13]

Another class of topological materials is materials with band gap inverted by strong spin-orbit interaction in which the topological surface states are protected by the crystal mirror symmetry [14] – so-called topological crystalline insulators (TCI). One representative of a TCI is SnTe , [15, 16] showing an even number of the Dirac cones in the surface spectrum.

Recently it was demonstrated that in the $\text{Bi}_2\text{Te}_3/\text{SnTe}$ heterostructure, the system containing \mathbb{Z}_2 and crystal mirror symmetry TIs, the $\bar{\Gamma}$ Dirac surface states of Bi_2Te_3 and SnTe annihilate at the interface while the Dirac state of SnTe at the \bar{M} “survives”. [17] This points out that the interaction of \mathbb{Z}_2 TI and TCI systems can results in unusual change in topological surface states picture.

Different systems, containing layers of band-inverted Bi_2Te_3 and SnTe materials are $(\text{SnTe})_n(\text{Bi}_2\text{Te}_3)_m$ compounds.[18] In this series the $(n = 1, m > 1)$ compounds – SnBi_4Te_7 , $\text{SnBi}_6\text{Te}_{10}$, and $\text{SnBi}_8\text{Te}_{13}$ are structurally identical to earlier studied lead-based TIs [10], containing alternating QL and SL structural units, while the $(n \geq 1, m = 1)$ compounds are formed by unique, nonalternating building blocks. The simplest system $(n = 1, m = 1)$, i.e. SnBi_2Te_4 is composed by SL hexagonally ordered blocks stacked along the c axis and separated by van der Waals spacings. The SL building block (Fig. 1(b)) can be obtained from the original QL block of Bi_2Te_3 (Fig. 1(a)) by introducing the SnTe bilayer between the Bi atomic layer and the central Te one. This compound was predicted to be 3D \mathbb{Z}_2 TI with single Dirac cone in the bulk energy gap [10]. The $\text{Sn}_2\text{Bi}_2\text{Te}_5$ compound $(n = 2, m = 1)$ is formed by nonuple layer (NL) building blocks [18]. The NL block (Fig. 1(c)) is constructed from SL block by introduction additional SnTe hexagonal bilayer in the middle of the SL or two bilayers into original QL. Thus this compound differs from $\text{Bi}_2\text{Te}_3/\text{SnTe}$ heterostructure having the ionic-covalent bonded Bi_2Te_3 and SnTe atomic layers. Another experimentally confirmed structure $(\text{SnTe})_n(\text{Bi}_2\text{Te}_3)_m$, which is also built from the ionic-covalent bonded Bi_2Te_3 and SnTe atomic layers is $\text{Sn}_3\text{Bi}_2\text{Te}_6$ $(n = 3, m = 1)$. [18] In this case additional SnTe layers are incorporated into the building block (Fig. 1(d)). We are not aware of the possibility of growth of stable $(\text{SnTe})_n(\text{Bi}_2\text{Te}_3)_{m=1}$ compounds with larger n which have building blocks of the same type.

In the present paper we demonstrate by means of relativistic density functional theory (DFT) calculations that $(\text{SnTe})_{n=2,3}(\text{Bi}_2\text{Te}_3)_{m=1}$ compounds are \mathbb{Z}_2 TIs, in which owing to complex band inversion of bulk states belonging to Bi_2Te_3 and SnTe subsystems at the surface arise the topological surface state (TSS) demonstrating non-Dirac, dog-leg dispersion within the bulk energy gap. We discuss the localization and spin texture of the TSS in the context of gate control of the topological transport properties. We also demonstrate the existence of such a TSS in $\text{Sn}_2\text{Sb}_2\text{Te}_5$ compound.

For calculations we use the Vienna Ab Initio Simulation Package (VASP) [19, 20] with generalized gradient approximation (GGA) [21] for the exchange correlation potential. The interaction between the ion cores and valence electrons was described by the projector augmented-wave method.[22, 23] Relativistic effects, including SOI, were taken into account. The atomic positions of bulk $(\text{SnTe})_{n=2,3}(\text{Bi}_2\text{Te}_3)$ compounds were optimized. In slab calculations a vacuum space of ~ 20 Å was included to ensure negligible interaction between opposite surfaces. Complementary calculations for bulk band structure were performed using the fullpotential linearized augmented plane-wave method as implemented in the FLEUR code.[24]

RESULTS

The bulk band structures of $\text{Sn}_2\text{Bi}_2\text{Te}_5$ shown in Fig. 2 have been calculated with and without SOI included. As can be seen from Fig. 2(a), the direct energy gap of 0.32 eV exist at the Γ point in the calculation without SOI which transforms into indirect gap of 0.12 eV under switch on the SOI (Fig. 2(b)). The time-reversal invariant momenta (TRIMs) in this Brillouin zone are the Γ , A and triply degenerate M and L points. We checked the parity of the

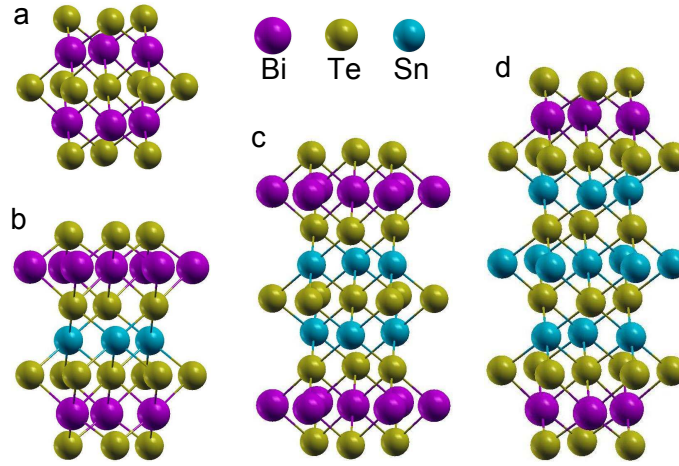


FIG. 1. (Color online) Building blocks of Bi_2Te_3 (a); SnBi_2Te_4 (b); $\text{Sn}_2\text{Bi}_2\text{Te}_5$ (c); and $\text{Sn}_3\text{Bi}_2\text{Te}_6$ (d).

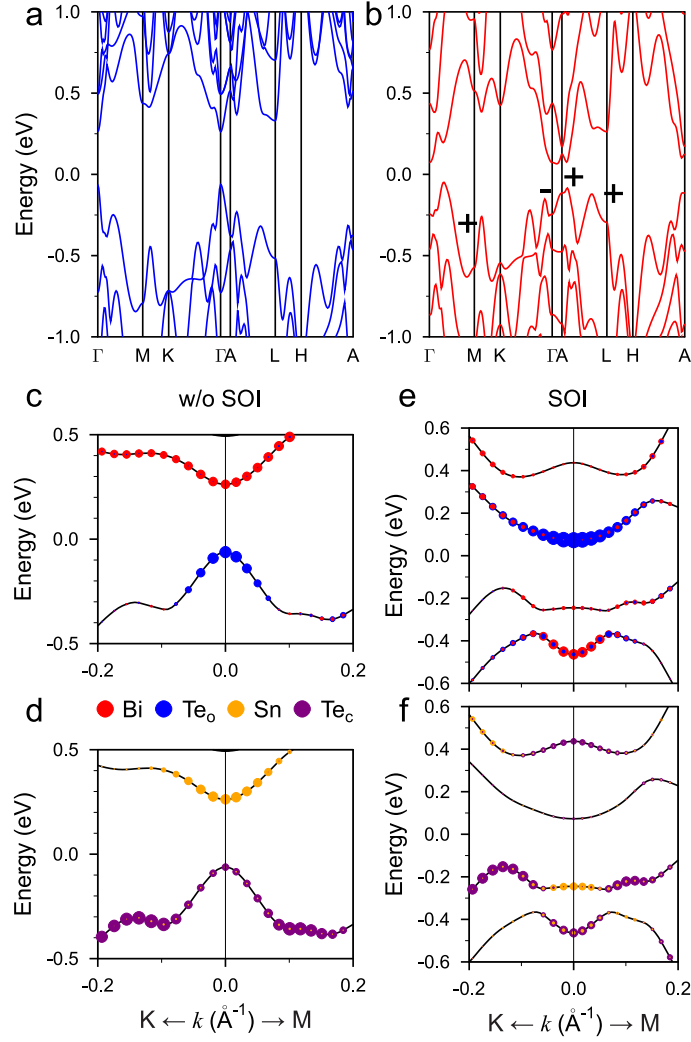


FIG. 2. (Color online) Bulk electronic structure of $\text{Sn}_2\text{Bi}_2\text{Te}_5$ calculated without (a) and with (b) SOI included (Signs of band parities at the TRIM are also shown). Atomic composition of the near-gap states in bulk $\text{Sn}_2\text{Bi}_2\text{Te}_5$ calculated without (c,d) and with (e,f) SOI included.

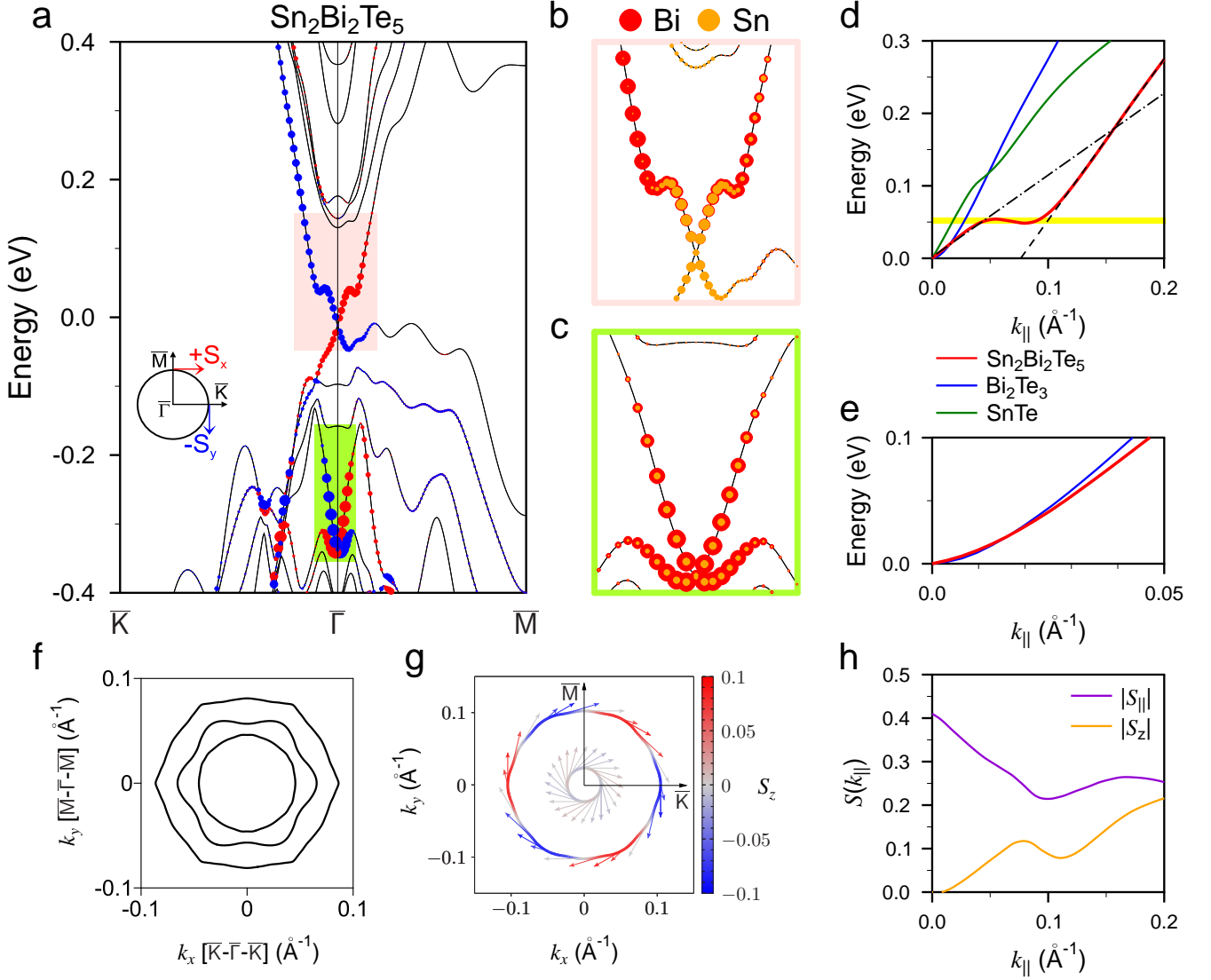


FIG. 3. (Color online) (a) Surface electronic structure of $\text{Sn}_2\text{Bi}_2\text{Te}_5$; The size of the color circles represent the weight of the states in the outermost building block (NL) of the slab; red and blue colors show the sign of the in-plane (S_x and S_y) spin components; lightpink and lightgreen rectangles mark the areas of the bandgap and valenceband topological surface states, respectively. Atomic weights of Bi and Sn in the bandgap (b) and valenceband (c) TSSs. (d) Energy dispersion of the bandgap TSS compared to Bi_2Te_3 and SnTe Γ Dirac cones. Dashed and dot-dashed lines are linear fit for the TSS above and below shoulder, respectively. (e) Dispersion of the valenceband TSS compared to Bi_2Te_3 . (f) Constant energy contours in the shoulder region (yellow stripe in panel (d)). (g) Spin-resolved constant energy contours for bandgap TSS at energies of 25 meV below and above the shoulders. Arrows adjacent to the contours denote the in-plane spin component S_{\parallel} . The out-of-plane spin component S_z is indicated by the color with red and blue corresponding to the positive and negative values, respectively. (h) The spin components S_{\parallel} and S_z for bandgap TSS as functions of k_{\parallel} along the Γ - \bar{K} direction.

wavefunctions at all TRIMs to determine the topological character of this material and found that the parity inversion of bulk bands occurs at the Γ point which leads to \mathbb{Z}_2 invariants 1;(000) like in Bi_2Te_3 .

In spite of this similarity in SOI-induced wavefunction parity change, the total band inversion at Γ is an entanglement of two different inversions corresponding to each subsystem due to the complex crystal structure of the compound. For instance, in Bi_2Te_3 the SOI modifies the top valence band state (predominantly of p_z character) of Te atoms lying in the outer layers of QL (Te_o) and the Bi p_z -state of the bottom conduction band so that they are inverted in the close vicinity of the Γ point. A similar simple band inversion occurs in the bulk SnTe where Sn and Te states are inverted in the L point of the cubic Brillouin zone. Instead, in $\text{Sn}_2\text{Bi}_2\text{Te}_5$ the spectra calculated without SOI both Bi and Sn states form the bottom of the conduction band while the states of Te_o atoms and tellurium atoms of the central

layer of NL (Te_c) lie in the top valence band (Fig. 2(c,d)). Switching on the SOI results in an inversion of Bi and Te_o states and Sn and Te_c states. However, in contrast to the binary systems this inversion has more complex character. As can be seen in Fig. 2(e) after switching on the SOI the Te_o states become dominant in the conduction band while the Bi states (in contrast to the Bi_2Te_3 case) occupy the second valence band in the vicinity of Γ . The SOI-inverted Sn states lie in the highest valence band and Te_c states appear in the second conduction band Fig. 2(f). Additionally, the SOI-inverted Sn states (with smaller weight) appear in the second valence band. Thus, the $\text{Sn}_2\text{Bi}_2\text{Te}_5$ TI has a competitive bulk Γ -gap band inversion which comprises the inversion of the states belonging to different subsystems, SnTe and Bi_2Te_3 , so that the valence band edge is mainly formed by Sn states and the conduction band edge occupied by Te_o states while the Bi and Te_c states lie next to the edges bands.

Such a superposition of the SOI-induced bulk band inversions in the the SnTe and Bi_2Te_3 subsystems of the $(\text{SnTe})_2(\text{Bi}_2\text{Te}_3)_1$ TI results in formation of unusual topological states on the surface. In the surface spectrum two topological surface states arise at the $\bar{\Gamma}$ point. The upper TSS lies in the band gap (see lightpink rectangle in Fig. 3a) while the lower TSS (lightgreen rectangle in Fig. 3a) resides in the valence band (bandgap and valenceband TSS's, respectively from now on). The lower, valenceband TSS, propagating within the local valence band gap, has typical Dirac dispersion for TIs. In contrast, the bandgap TSS displays nonlinear (non-Dirac) dog-leg behavior. It has two linear sections in the spectrum: near the band crossing (Dirac point) and below the conduction band which connect to each other in the middle part of the gap with formation of shoulders in the spectrum. Like in other TIs, the TSSs in $\text{Sn}_2\text{Bi}_2\text{Te}_5$ are localized within outermost building block of the slab. However, in this case, where the building block has two band-inverted SnTe and Bi_2Te_3 subsystems, the localization of the TSS is affected by the peculiarities in the bulk band inversion. Figs. 3(b,c) show the Bi and Sn atomic weights in the TSSs. As one can see in Fig. 3(c), the valenceband TSS has dominant Bi weights that reflect its dominant localization in the outer Bi-Te layers of NL. Comparing the dispersion of this state with that of the Dirac cone in Bi_2Te_3 [8] (Fig. 3(e)) one can conclude that at small k_{\parallel} (where the valenceband TSS has localized character) both bands are almost identical. In the bandgap TSS (Fig. 3(b)), the lower linear section near the band crossing, the Sn contribution dominates and thus the state is mainly localized in the inner Sn-Te layers of NL. Approaching the shoulders the Sn contribution disappears rather quickly and above the band shoulders the TSS becomes to be mostly localized in the outer Bi-Te layers. Thus the band shoulders in the TSS spectrum are associated with the change of the TSS localization from the SnTe to Bi_2Te_3 subsystem. It should be noted that the slope of the upper linear section of the bandgap TSS (at $k_{\parallel} > 0.1 \text{ \AA}^{-1}$) localized in the outer Bi-Te layers is comparable with the slope of the Bi_2Te_3 Dirac cone (Fig. 3(d)), while the dispersion of the lower linear section ($k_{\parallel} < 0.05 \text{ \AA}^{-1}$) differs considerably from both Bi_2Te_3 and rocksalt-SnTe[25] $\bar{\Gamma}$ Dirac states. As a consequence, the linear fitting for lower and upper sections of the bandgap TSS (dot-dashed and dashed lines in Fig. 3(d)) gives E/k_{\parallel} slopes of 2.22 and 1.13, respectively. Between these linear sections, in the shoulder region at $0.05 < k_{\parallel} < 0.1 \text{ \AA}^{-1}$, two inflection points exist which limit almost flat section in the TSS spectrum. Such very low velocity regime in the bandgap TSS resembles heavy-fermion topological state that has been proposed theoretically[26] and obtained from magnetothermoelectric transport measurements[27] in topological Kondo insulator (TKI) SmB_6 . Owing to slightly negative dispersion of the TSS in the shoulder region (see narrow yellow stripe in Fig. 3(d)) by varying the chemical potential the system will pass from one velocity mode in the lower linear section to the other velocity mode in the upper linear section through the three surface Fermi pockets regime at energy $\approx 50 \text{ meV}$ (Fig. 3(f)).

The detailed spin texture of the bandgap TSS is illustrated in Figs. 3(g,h). Fig. 3(g) shows spin-resolved constant energy contours (CEC's) for the lower (inner contour) and upper (outer contour) linear sections of the TSS. Both contours, apart from the in-plane clockwise spin polarization, also demonstrate the presence of the out-of-plane spin component, which is intrinsic feature of the spin-polarized states at hexagonal surfaces while S_z for the inner contour is extremely small. As clearly seen for the outer contour, S_z is zero along $\bar{\Gamma}$ - \bar{M} and reaches a minimum (maximum) value in $\bar{\Gamma}$ - \bar{K} directions. The dependencies of absolute values for S_{\parallel} and S_z on k_{\parallel} along $\bar{\Gamma}$ - \bar{K} are shown in Fig. 3(h). The in-plane spin polarization having maximum near the band crossing point rapidly decreases approaching the shoulder. At $k_{\parallel} > 0.1 \text{ \AA}^{-1}$, i.e. in the upper linear section, it increases with k_{\parallel} until it reaches the region of the bulk states. In contrast, the out-of-plane spin polarization increases with k_{\parallel} in both linear sections of the TSS, having a kink at the band shoulder.

The increase of the SnTe layers in the building block of $(\text{SnTe})_n(\text{Bi}_2\text{Te}_3)_{m=1}$ compound up to $n = 3$ maintains the two TSSs in the surface spectrum as well as dog-leg behavior in dispersion of the bandgap surface state (Fig. 4(a)). The difference from the $\text{Sn}_2\text{Bi}_2\text{Te}_5$ case is that the band shoulders lie closer to the bulk valence band making lower section of the TSS very short and two times less steep.

Another way to modify the parameters of the bandgap TSS is substitution of Bi by Sb. In this case SnTe layers are introduced into Sb_2Te_3 TI forming $(\text{SnTe})_n(\text{Sb}_2\text{Te}_3)_{m=1}$ compound. As can be seen in Fig. 4(b) the surface spectrum

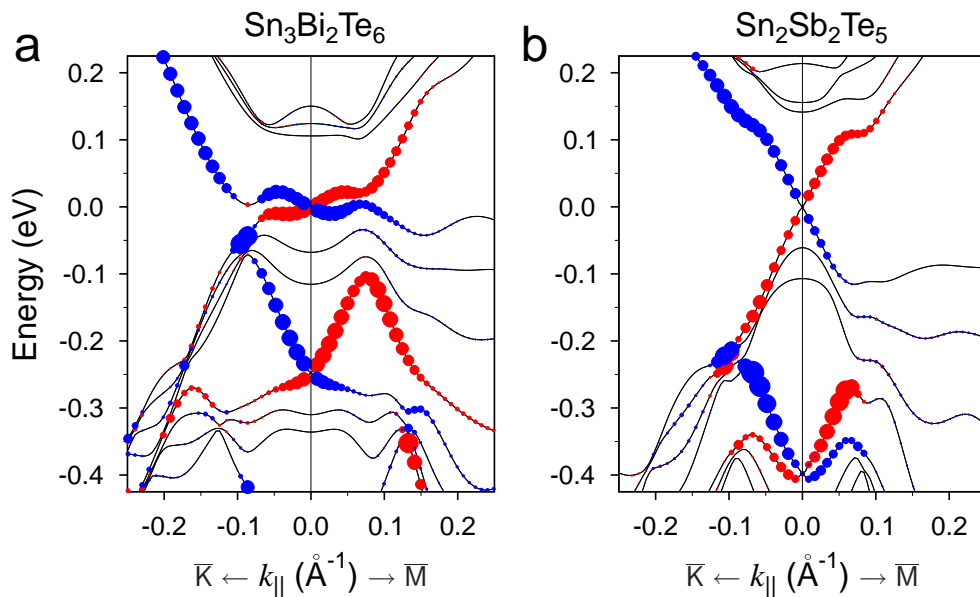


FIG. 4. (Color online) Spin-resolved surface electronic structure of $\text{Sn}_3\text{Bi}_2\text{Te}_6$ (a) and $\text{Sn}_2\text{Sb}_2\text{Te}_5$ (b).

of $\text{Sn}_2\text{Sb}_2\text{Te}_5$ also holds two TSSs with dog-leg dispersion in the bandgap TSS. However, in contrast to the previous case the band shoulders arise near the conduction band.

SUMMARY

In summary, on the basis of *ab initio* DFT calculations we have demonstrated that $(\text{SnTe})_{n=2,3}(\text{Bi}_2\text{Te}_3)_{m=1}$ compounds are \mathbb{Z}_2 topological insulators in which, owed to superposition of two pairs of SOI-induced band inversions realized in SnTe and Bi_2Te_3 subsystems, two spin-helical topological surface states arise at the $\bar{\Gamma}$ point. These states reside in the band gap and in the local gap of the valence band. The latter TSS, lying deep below the Fermi level, has a dispersion similar to that in the Bi_2Te_3 TI, while the bandgap TSS demonstrates unusual non-Dirac dog-leg dispersion with two linear sections of different slope and very low-velocity shoulder section between them. In $\text{Sn}_2\text{Bi}_2\text{Te}_5$ the shoulders are located in the middle of the gap and velocities of carriers in lower and upper linear sections differ by a factor of two. Thus in contrast to all hitherto known TIs, where the slope of the spin-helical TSS is linear or varies smoothly with energy, the bandgap TSS in $(\text{SnTe})_{n=2,3}(\text{Bi}_2\text{Te}_3)_{m=1}$ compounds shows abrupt switch of the velocity of topological carriers with change in the Fermi surface topology in the narrow energy range (shoulder section) where spin and charge current should be blocked. We also demonstrated that similar TSSs exist in $(\text{SnTe})_{n=2}(\text{Sb}_2\text{Te}_3)_{m=1}$ compound. This novel finding enhance the understanding on the diversity of topological surface states and pave a way for the efficient control of the group velocity with sufficiently large spin current density by tuning the chemical potential.

Further tuning of the bandgap TSS parameters can be realized by using $(\text{Bi}_{1-x}\text{Sb}_x)_2\text{Te}_3$ [28, 29] or $\text{Bi}_2(\text{Te}_{1-x}\text{Se}_x)_3$ [29, 30] compounds as basic TIs for construction of $(\text{SnTe})_n((\text{Bi-Sb})_2(\text{Te-Se})_3)_{m=1}$ systems.

-
- [1] Y. Xia, D. Qian, D. Hsieh, L. Wray, A. Pal, H. Lin, A. Bansil, D. Grauer, Y. S. Hor, R. J. Cava, and M. Z. Hasan, *Nature Physics* **5**, 398 (2009).
 - [2] Y. L. Chen, J. G. Analytis, J.-H. Chu, Z. K. Liu, S.-K. Mo, X. L. Qi, H. J. Zhang, D. H. Lu, X. Dai, Z. Fang, S. C. Zhang, I. R. Fisher, Z. Hussain, Z.-X. Shen, *Science* **325**, 178 (2009).
 - [3] Tong Zhang, Peng Cheng, Xi Chen, Jin-Feng Jia, Xucun Ma, Ke He, Lili Wang, Haijun Zhang, Xi Dai, Zhong Fang, Xincheng Xie, and Qi-Kun Xue, *Phys. Rev. Lett.* **103**, 266803 (2009).
 - [4] K. Kuroda, M. Arita, K. Miyamoto, M. Ye, J. Jiang, A. Kimura, E. E. Krasovskii, E. V. Chulkov, H. Iwasawa, T. Okuda, K. Shimada, Y. Ueda, H. Namatame, and M. Taniguchi, *Phys. Rev. Lett.* **105**, 076802 (2010).
 - [5] H. Zhang, C.-X. Liu, X.-L. Qi, X. Dai, Z. Fang, and S.-C. Zhang, *Nature Phys.* **5**, 438 (2009).

- [6] W. Zhang, W. Yu, H.J. Zhang, X. Dai, and Z. Fang, *New J. Phys.* **12**, 065013 (2010).
- [7] Y. Zhang, K. He, C.-Z. Chang, C.-L. Song, L.-L. Wang, X. Chen, J.-F. Jia, Z. Fang, X. Dai, W.-Y. Shan, S.-Q. Shen, Q. Niu, X.-L. Qi, S.-C. Zhang, X.-C. Ma, and Q.-K. Xue, *Nature Phys.* **6**, 584 (2010).
- [8] S.V. Eremeev, Yu.M. Koroteev, E.V. Chulkov, *JETP Lett.* **91**, 387 (2010).
- [9] K. Eto, Z. Ren, A.A. Taskin, K. Segawa, and Y. Ando, *Phys. Rev. B* **81**, 195309 (2010).
- [10] S.V. Eremeev, G. Landolt, T. V. Menshchikova, B. Slomski, Y. M. Koroteev, Z. S. Aliev, M. B. Babanly, J. Henk, A. Ernst, L. Patthey, A. Eich, A. A. Khajetoorians, J. Hagemeyer, O. Pietzsch, J. Wiebe, R. Wiesendanger, P. M. Echenique, S. S. Tsirkin, I. R. Amiraslanov, J. H. Dil, E. V. Chulkov, *Nature Commun.* **3**, 635 (2012).
- [11] K. Kuroda, H. Miyahara, M. Ye, S. V. Eremeev, Yu. M. Koroteev, E. E. Krasovskii, E. V. Chulkov, S. Hiramoto, C. Moriyoshi, Y. Kuroiwa, K. Miyamoto, T. Okuda, M. Arita, K. Shimada, H. Namatame, M. Taniguchi, Y. Ueda, A. Kimura, *Phys. Rev. Lett.* **108**, 206803 (2012).
- [12] M. Neupane, S.-Y. Xu, L.A. Wray, A. Petersen, R. Shankar, N. Alidoust, Chang Liu, A. Fedorov, H. Ji, J.M. Allred, Y.S. Hor, T.-R. Chang, H.-T. Jeng, H. Lin, A. Bansil, R.J. Cava, and M.Z. Hasan, *Phys. Rev. B* **85**, 235406 (2012).
- [13] Taichi Okuda, Takamasa Maegawa, Mao Ye, Kaito Shirai, Takuya Warashina, Koji Miyamoto, Kenta Kuroda, Masashi Arita, Ziya S. Aliev, Imamaddin R. Amiraslanov, Mahammad B. Babanly, Evgueni V. Chulkov, Sergey V. Eremeev, Akio Kimura, Hirofumi Namatame, and Masaki Taniguchi, *Phys. Rev. Lett.* **111**, 206803 (2013).
- [14] L. Fu, *Phys. Rev. Lett.* **106**, 106802 (2011).
- [15] T. H. Hsieh, H. Lin, J. Liu, W. Duan, A. Bansil, and L. Fu, *Nat. Commun.* **3**, 982 (2012).
- [16] Y. Tanaka, Z. Ren, K. Nakayama, S. Souma, T. Takahashi, K. Segawa, and Y. Ando, *Nat. Phys.* **8**, 800 (2012).
- [17] Tomáš Rauch, Markus Flieger, Jürgen Henk, and Ingrid Mertig, *Phys. Rev. B* **88**, 245120 (2013).
- [18] B.A. Kuropatwa and H. Kleinke, *Z. Anorg. Allg. Chem.* **638**, 2640 (2012).
- [19] G. Kresse, J. Hafner, *Phys. Rev. B* **48**, 13115 (1993).
- [20] G. Kresse, J. Furthmüller, *Comput. Mater. Sci.* **6**, 15 (1996).
- [21] J.P. Perdew, K. Burke, M. Ernzerhof, *Phys. Rev. Lett.* **77**, 3865 (1996).
- [22] P.E. Blöchl, *Phys. Rev. B* **50**, 17953 (1994).
- [23] G. Kresse, D. Joubert, *Phys. Rev. B* **59**, 1758 (1999).
- [24] [<http://www.flapw.de>]
- [25] S.V. Eremeev, Yu.M. Koroteev, I.A. Nechaev, and E.V. Chulkov, *Phys. Rev. B* **89**, 165424 (2014).
- [26] V. Alexandrov, M. Dzero, and P. Coleman, *Phys. Rev. Lett.* **111**, 226403 (2013).
- [27] Yongkang Luo, Hua Chen, Jianhui Dai, Zhu-an Xu, and J. D. Thompson, *Phys. Rev. B* **91**, 075130 (2015).
- [28] Jinsong Zhang, Cui-Zu Chang, Zuocheng Zhang, Jing Wen, Xiao Feng, Kang Li, Minhao Liu, Ke He, Lili Wang, Xi Chen, Qi-Kun Xue, Xucun Ma, and Yayu Wang, *Nature Commun.* **2**, 574 (2011).
- [29] Z. Ren, A.A. Taskin, S. Sasaki, K. Segawa, and Y. Ando, *Phys. Rev. B* **84**, 165311 (2011).
- [30] A. M. Shikin, I. I. Klimovskikh, S. V. Eremeev, A. A. Rybkina, M. V. Rusinova, A. G. Rybkin, E. V. Zhizhin, J. Sanchez-Barriga, A. Varykhalov, I. P. Rusinov, E. V. Chulkov, K. A. Kokh, V. A. Golyashov, V. Kamyshlov, and O. E. Tereshchenko, *Phys. Rev. B* **89**, 125416 (2014).